


## Article

# A Novel Method for Joining Steel/Al Tube Parts Based on Electromagnetic Force by Flat Coil

Quanxiaoxiao Liu, Yuanheng Yao, Zehua Xia, Guangyao Li, Junjia Cui  and Hao Jiang \* 

State Key Laboratory of Advanced Design and Manufacturing for Vehicle Body, Hunan University, Changsha 410082, China; lqxxwkk@hnu.edu.cn (Q.L.); yaoyuanheng@hnu.edu.cn (Y.Y.); XiaZeHua@saicmotor.com (Z.X.); zoe122208@163.com (G.L.); cuijunjia@hnu.edu.cn (J.C.)

\* Correspondence: haojiang@hnu.edu.cn; Tel.: +86-731-8866-4001; Fax: +86-731-8882-2051

**Abstract:** Electromagnetic joining technology is an effective technique to join tubes with dissimilar materials. In this paper, a new approach for steel/Al tube parts joined by electromagnetic crimping using a flat coil was investigated. Electromagnetic crimping process experiments with different discharge energies (12, 14, and 16 kJ) and property tests were carried out. Meanwhile, the deformation characteristics of the outer tube under different discharging energies were discussed to study the fittability of the joining zone. The quality of the crimped joint was analyzed by microstructure characterization. The results show that the proposed approach was able to obtain torque joints and was potentially for tubular parts manufacturing. Moreover, higher discharging energy would result in better fittability degree and torque strength but might cause some cracks in the necking area. Combining the results of torsion tests with the microstructure observation, the comprehensive performance of the joint formed under a moderate discharge energy (14 kJ) was optimal.

**Keywords:** electromagnetic crimping; steel/Al; tube-parts connections; microstructure



**Citation:** Liu, Q.; Yao, Y.; Xia, Z.; Li, G.; Cui, J.; Jiang, H. A Novel Method for Joining Steel/Al Tube Parts Based on Electromagnetic Force by Flat Coil. *Coatings* **2021**, *11*, 1356. <https://doi.org/10.3390/coatings11111356>

Academic Editor: Annalisa Fortini

Received: 16 September 2021

Accepted: 28 October 2021

Published: 3 November 2021

**Publisher's Note:** MDPI stays neutral with regard to jurisdictional claims in published maps and institutional affiliations.



**Copyright:** © 2021 by the authors. Licensee MDPI, Basel, Switzerland. This article is an open access article distributed under the terms and conditions of the Creative Commons Attribution (CC BY) license (<https://creativecommons.org/licenses/by/4.0/>).

## 1. Introduction

Reducing vehicle weight can effectively improve the mileage of new energy vehicles. A direct and efficient way to reach the target of lightweight design is the substitution of low-density but high-strength materials like aluminum, magnesium, fiber-reinforced composite materials for steel [1–3]. One innovative concept of lightweight designs is so-called smart structures, in the manufacturing of which is often required to join tubes with different materials. However, the joining of parts in different materials is a challenging task. Some conventional joining techniques are not suitable for making high-quality joints [4–6]. As a result, many researchers have focused on searching for new methods.

Joining processes based on plastic deformation of at least one joining part promised great potential regarding the production of multi-material joints [7]. The use of plastic deformation for joining parts potentially offered improved accuracy, reliability, and environmental safety as well as creating opportunities to design new products through joining dissimilar materials [8]. Joining plastic deformation for tubes mainly has the following several ways. For instance, in the friction stir welding (FSW) process, materials around the interface are heated by friction between continuously moving surfaces, and then the force is applied to cause large plastic deformation for bonding the surfaces. According to Chen et al. [9], small-dimension Al 3003 pipe and pure copper pipe of the thin wall (Al: 1.5 mm; Cu: 1 mm) and small diameter (19 mm) were successfully joined by a developed welding method with a specially-designed friction stir welding (FSW) system. Moreover, joining by mechanical crimping was developed in 1930 to join couplings onto hydraulic hoses, which used segmented tools and was still the major application of this process [10]. Shirgaokar et al. [11] used mechanical crimping to join tubular parts without an intermediate plastic or rubber tube. The influence of workpiece positioning, press jaw movement, and tool geometry on the pull-out force and the material thinning in the joint zone were

examined. In contrast to mechanical crimping, joining by hydraulic crimping uses an elastomer to apply the required forming pressure on the surface of the workpiece to make a joint [12].

An alternative technique for joining dissimilar materials by plastic deformation is driven by electromagnetic force, which uses pulsed magnetic fields to form highly conductive metals at a high speed. Magnetic pulse welding (MPW), as it is known, is one of these cases. The typical setup of MPW consists of the EMF machine, tool coil, and workpiece. This setup can be represented by an RLC circuit in which the forming machine is symbolized by the inner resistance  $R_i$ , the inner inductance  $L_i$  and the capacitance  $C$ . The combination of tool, coil, and workpiece is considered to be the consumer load of the circuit. Compared to other welding technologies, the process of MPW is environmentally friendly for no emission of heat, radiation, gas, or smoke during the process, which provides safer and cleaner conditions for the operator. It allows the joining of dissimilar material combinations, keeping their mechanical and chemical properties intact quickly and cost-effectively [13]. Time-consuming post-weld activities like cleaning and finishing are not required.

Electromagnetic crimping is another process variant, whose principle is similar to MPW. For the manufacturing of crimping connections, the material of one joining part is formed into an undercut of the other partner. Thereby, an interlock, which ensures the load transfer between both parts is generated [14–16]. Based on its characteristics, many researchers have studied electromagnetic crimping technology. For example, Golovashchenko [17] examined the influence of circumferential grooves geometries on the achievable push-out strength. The results showed that when the tube wall just touched the bottom of the groove, the push-out force was increased with a decreasing groove width and an increasing groove depth. Park et al. [18] analyzed the influence of geometric parameters on joint strength through simulations and experiments. Different from the study of Golovashchenko [17], they used the same charging energy in all of their experiments and observed an increase in the transferable load with an increasing width and depth. Based on these results, axial and torque joint were designed and guidelines for designing crimped joints were established. In addition, Weddeling et al. [19] studied the influence of groove shapes (rectangular, circular, and triangular) on the pull-out force. It was found that higher deformation/higher stiffness in the tube was existed due to the mandrel groove geometry, smaller resulting angle, and partial shearing at the groove edge. To facilitate the connection design, Weddeling et al. [20] further presented an analytical approach for the prediction of the joining zone parameters with respect to the loads to be transferred. The experimental studies in which groove dimensions and their shape were major parameters regarding the load transfer under quasi-static tension are performed to validate the approach. Then they developed design strategies and a process window for the manufacturing of such crimped joints. The studies of electromagnetic crimping mentioned above mainly used the typical setup of tube compression processes, and most of current investigations and publications dealing with crimped joints focused on the groove dimensions. However, the present electromagnetic crimping method for pipe fittings is to use a circular magnetic collector. A magnetic collector of one diameter can only connect pipe fittings of the corresponding diameter. This kind of electromagnetic crimping requires the replacement of magnetic collectors when joining the tubes with different diameters, and the cost is high. Therefore, a novel method is proposed to connect pipe fittings of different diameters without changing the coil.

In this paper, a new approach for electromagnetic tube-parts connections was proposed. A flat coil was used for the manufacturing of torque joints. In this way, it becomes more convenient and flexible for the industrial application of electromagnetic crimping, and only one tool coil is enough to be used for tubes with various diameters. Moreover, in the case where a single connection of large energy cannot be achieved due to the discharge energy limitation of the device, a multi-step connection under small energy can be realized based on the new approach.

## 2. Materials and Methods

### 2.1. Novel Electromagnetic Crimping Method

Figure 1 presents the schematic of the novel electromagnetic crimping process. The inner tube designed six grooves on the surface which are uniformly arranged on its surface. The coil was in the traditional flat form. The setup for electromagnetic crimping and the size of specimens are shown in Figure 2. A transient magnetic field is produced when a discharge current of a high-frequency sinusoidal wave flows through a coil. This transient magnetic field leads to eddy currents in the surface of the outer tube which is close to the coil. According to Faraday's law of induction, a repulsive force occurs between the coil and outer tube [21]. When the material's yield strength is exceeded, the repulsive force acting on the outer tube causes a plastic deformation. Then the outer tube deforms inwardly at a high velocity into a groove on the outer surface of the inner tube to obtain joining. Thus, the first connected part of the crimped joint is formed. Besides, as described above, an insulating film of a certain thickness is arranged between the coil and the outer tube. To prevent the joint from moving in the direction perpendicular to the plane of the coil under the electromagnetic force, the connecting area is pressed by a specific part (insulated bakelite). The gap between the outer tube and the coil is 0.5 mm.

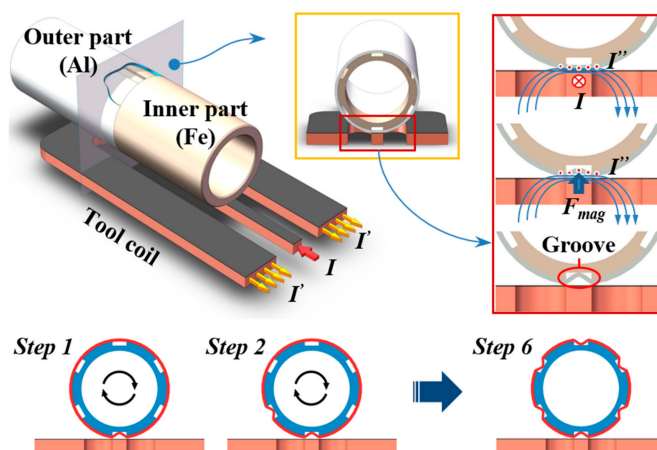


Figure 1. Schematic of electromagnetic crimping using a flat coil.

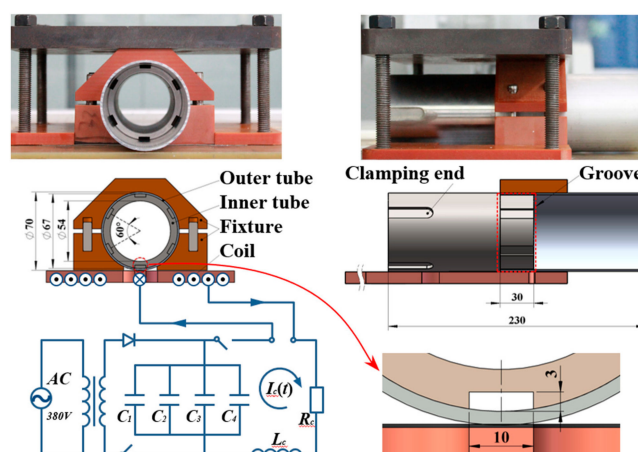


Figure 2. Setup for electromagnetic crimping and the size of specimens (dimensions in mm).

Then, when the first groove is connected, the joint carried on a rotatable support rotates at a defined angle (rotating arrow in Figure 1). The coil is subsequently energized to drive the next region of the outer tube to form into another groove. This process is then repeated until a desired number of the connected part is finished.

The magnetic pulse generator (PST, Alzenau, Germany) with a capacitance of 408  $\mu\text{F}$  and a maximum charging voltage of 16 kV was used for providing discharge energy. A flat coil with a minimal cross-position of 10 mm  $\times$  10.5 mm was used as a joining tool. To investigate the influence of process parameters on the joint strength, discharge energies of 12–16 kJ with an interval of 2 kJ were used. For all pipe joints, each of the six grooves on the same inner tube was formed from a self-locking with the outer tube under the same charging energy.

## 2.2. Materials Preparation

AA 6061 T6 aluminum alloy (Chinalco, Beijing, China) with a thickness of 1.5 mm was used for the outer tube, and #45 hot rolling carbon construction steel (Baosteel, Shanghai, China) was selected as the inner tube. All specimens had a length of 130 mm. The properties of the materials are shown in Table 1. The groove width, length, and depth were manufactured at 10.0, 30.0, and 3.0 mm, respectively. To remove potential contaminations from preceding manufacturing and handling processes from the specimen's surfaces, the tubes were cleaned in an ultrasonic bath (GT SONIC, Meizhou, China) filled with acetone for at least 5 min. In this way, the same surface conditions for all specimens could be ensured.

**Table 1.** Properties of the materials.

Material	Density [g/cm <sup>3</sup> ]	Electrical Conductivity [MS/m]	Thermal Conductivity [W/(m·K)]	Yield Stress [MPa]
AA 6061	2.7	22–30	170–200	240
#45 steel	7.85	4	50.2	355

## 2.3. Test Methods

Torsion tests under quasi-static loading rate were carried out to evaluate the joining strength of the joints. Three repeated samples were tested at each discharge energy. During the test process, the end parts of the inner and outer tube were fixed on the clamping heads on both sides of the machine respectively. The clamping chuck connected with the inner tube was kept at rest, and the clamping chuck connected with the outer tube rotated at speed of 10°/min, as shown in Figure 3. Microstructure observations were carried out with an Olympus polarizing microscope (Olympus, Tokyo, Japan). Figure 4 shows the position of the microscopic observation, the connection area was divided into 7 positions on average in the  $x$ -axis direction (position A–G), then each position was cut away by wire cutting.

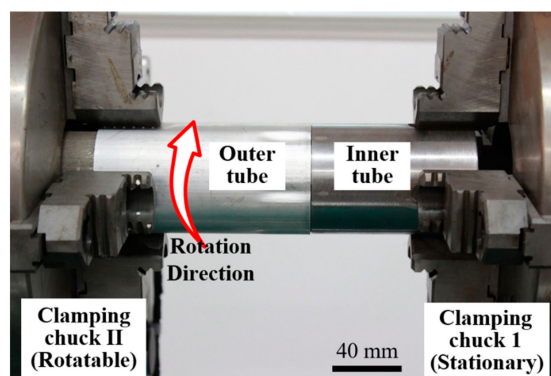


**Figure 3.** The setup of torsion tests.

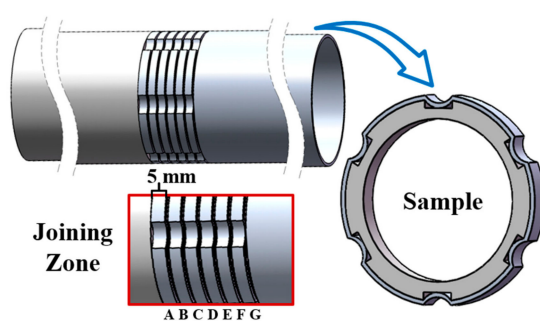


Figure 4. Specimen of microscopic observation.

### 3. Results and Discussion

#### 3.1. Torsional Strength and Failure Modes

Figure 5 shows three typical torque-angle curves of the pipe electromagnetic crimped joints under different discharge energies. It could be found that the torsional strength of the joint under 12 kJ was obviously lower than that of joints under another two energies. While the trend of the joint with 14 and 16 kJ was similar. At first, the torque increased approximately linearly with the increase in the angle of rotation. When the torsion angle was about  $15^\circ$ , the torsion force of the joint with 12 kJ reached its peak (about 1200 N.m). Subsequently, its value decreased rapidly with the increase of the torsion angle. As for the joint with discharge energies of 14 and 16 kJ, the torsion angles reaching the peak (about 1650 N.m) were delayed at about  $26^\circ$ , and then they fell more slowly than the joint with 12 kJ.

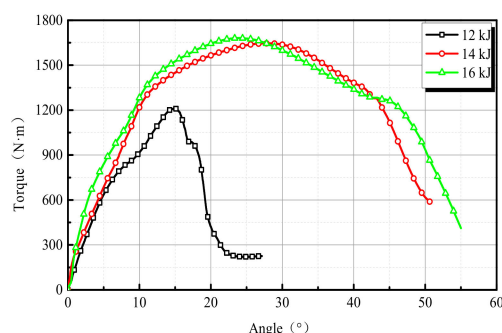
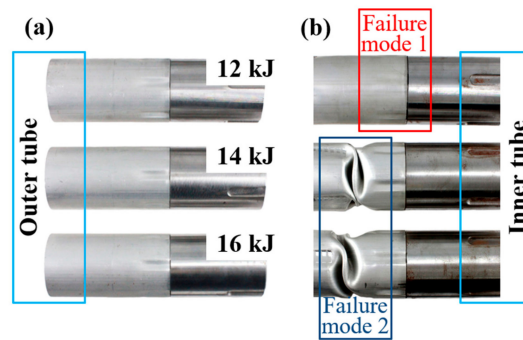


Figure 5. Torque force-angle curve of electromagnetic crimped joints formed under different discharge energies.

Figure 6 shows the specimens before and after the torsion test. It could be seen that the outer tube was mainly deformed, and two failure modes were observed during the torsion test. At the discharge energy of 12 kJ, the outer tube twisted out of the groove (called failure mode 1). This was because the discharge energy was small, and the forming force was insufficient. There was not enough interlock between the outer tube and groove to withstand the torque. At the discharge energy of 14 and 16 kJ, severe distortion occurred at the outer tube (failure mode 2). This indicated a relatively higher degree of interlock between the outer tube and groove.





**Figure 6.** Samples of the electromagnetic crimping joints: (a) after process experiments; (b) after torsion tests.

Figure 7 shows the torsional process of the two failure modes during the torque test. Based on the final failure position, three typical torsional angles were selected. It basically represented two stages: one was that the torque increases from zero to maximum, another was torque decreasing. Wherein  $\varphi$  was the angle the outer tube rotated relative to the inner tube in the connected zone. At the first stage, it could be seen that the outer tube rotated at a small angle during the torque test for both failure modes, and the  $\varphi_1$  value of failure mode 1 was a little bigger than that of failure mode 2. This indicated that the outer tube was mainly distorted and the dislocation in the groove was small. At the second stage, the  $\varphi_2$  value of failure mode 1 was much bigger than that of failure mode 2. This illustrated that the two tubes for failure mode 1 had a larger dislocation at the stage.

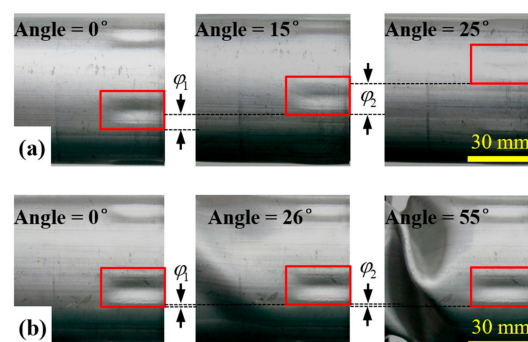


**Figure 7.** Torsional process of the joint: (a) failure mode 1 (the discharge energy of 12 kJ), and (b) failure mode 2. (the discharge energy of 16 kJ).

In a word, during the torsion test process, when the torque was small, the outer tube was elastically deformed. At this stage, the torque was approximately linearly increased with respect to the rotation angle. When the strength of the interlock was lower than the strength of the outer tube parent material, the interlock would be deformed with the increased torque, to be twisted out from the groove (failure mode 1). While the strength of the interlock was higher than the strength of the outer tube parent material, distortion occurred on the outer tube parent material (failure mode 2).

### 3.2. Fittability of Joining Zone

To obtain a high-quality crimped joint, it is important to ensure the consistency of the deformation of the outer tube on both sides of the groove. Figure 8 shows the cross-section observation of the joints at position D (see Figure 4). It could be clearly seen that the outer tube wall filled the groove of the inner tube under the action of the electromagnetic force, and a gap between the inner wall of the outer tube and groove base could be observed as well. The deformation of the outer tube was symmetrical with respect to the centerline of the groove under different discharge energy, and the maximum deformation of the outer

tube increased with the increasing discharge energy. The outer tube wall made contact with the groove base when the discharging energy was 16 kJ. The shearing and necking near the edge of the groove could be seen clearly as well.

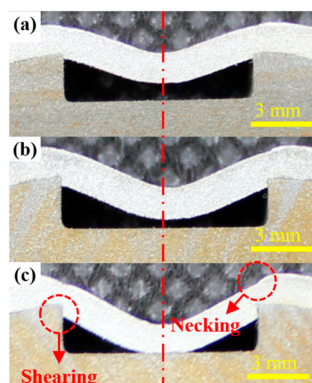


**Figure 8.** The deformation of the outer tube at position D (a) under 12 kJ, (b) 14 kJ, and (c) 16 kJ.

The above test results showed that the strength of the joints with 14 and 16 kJ was higher than that of 12 kJ. It could be attributed to that the increase in discharging energy resulting in increasing deformation of the outer tube to fill the groove. Greater resistance could be provided during the torsion process. In addition, the deformation of the outer tube was different in the groove, so the specific deformation value was measured as shown in Figure 9. It could be found that the maximum deformation of different positions in the axial direction of the joint formed under various discharge energies was different. The deformation of the outer tube in the middle position of the connecting area (position D) was the biggest and gradually decreased from the middle to the two sides. The overall deformation near the inner tube side (region from position A to position D) was bigger than that away from the inner tube side (region from position D to position G) in the connected area. This was mainly due to the difference in the maximum deformation between position A and position G. There were two main reasons for this difference: one was the difference of the constraint imposed on between position A and G. It could be seen that position A was a free end while position G was not, which made it easier for position A to deform. Another was that position G was located on the edge of the coil, and the cross-positional area of the coil at the location of position G differed from that at the location of position A. The electromagnetic forces experienced by the outer tube wall at position G was lower than that at position A. As for the reason why position G was located on the edge of the coil, it was because without a mandrel supporting inside the outer tube. If the position of the connection region was moved toward the side away from the coil edge, the region closed to the connected area on the outer tube would be deformed by electromagnetic force, which would affect the joint quality.

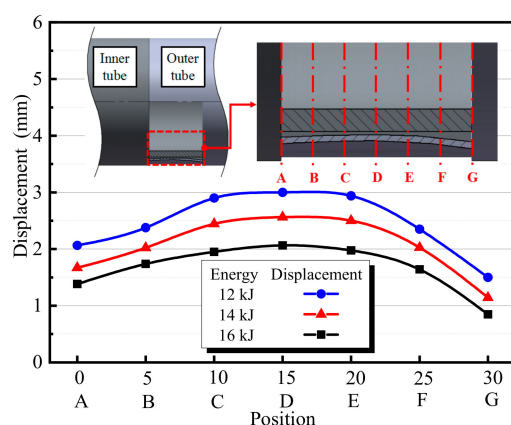


**Figure 9.** The maximum deformation of the outer tube at various positions under different discharge energies.

However, the strength of the joint did not increase as the energy increased continuously, because of the existing thinned area (the partial shearing of the tube at the groove edge) as proved by Weddeling et al. [19]. The thinning of the tube due to shearing at the groove edge would weaken the joint more than the strength increase seen by forming the tube into a groove, to cause overall joint strength to decrease. As for the shearing of the tube, they also pointed out that the effects of shearing played a prominent role in the strength of the joint. In this study, a geometric analysis model was established to investigate the degree of shearing and necking of the outer tube under different discharge energy, as shown in Figure 10.

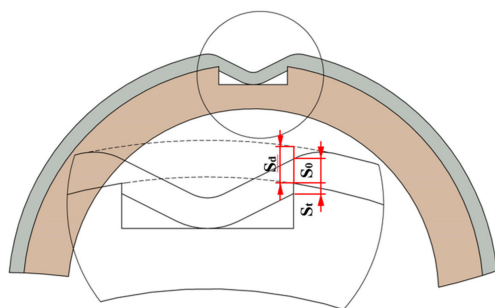


**Figure 10.** Schematic of the geometric analysis model.

The shearing rate is defined as

$$t_{shearing} = \frac{S_{\tau}}{S_0} \times 100\% \quad (1)$$

The necking rate is defined as

$$t_{necking} = \frac{S_0 - S_d}{S_0} \times 100\% \quad (2)$$

where  $S_0$  is the original thickness of the outer tube,  $S_d$  is the minimum wall thickness of the necked area in the direction of the sidewall of the groove, and  $S_{\tau}$  is the shearing displacement in the direction of the sidewall of the groove. The values of  $S_0$ ,  $S_d$ , and  $S_{\tau}$  were measured under the microscope, which were averaged from the value of three repeated samples under one discharge energy.

Figure 11 illustrates the shearing and necking rate distribution of the outer tube wall at different cross-positions under three discharge energies. It could be seen from Figure 11a that the shearing rate of the outer tube wall in each position increased with the increase of



discharge energy. The shearing rates at the middle of the connected area (from position C to position E) changed more obviously with the increase of discharge energy. Moreover, before the tube wall made contact with the groove base, where the outer tube wall was deformed large, the shearing rate at the groove edge was large. However, after the tube wall reached the groove base, the degree of the shearing rate changed less. The shearing rates of the different positions of the joint formed under the same discharge energy were greater as the energy increased. This indicated that the position had a greater influence on the shear rate. A similar trend occurred in the necking rate of the outer tube, as shown in Figure 11b.

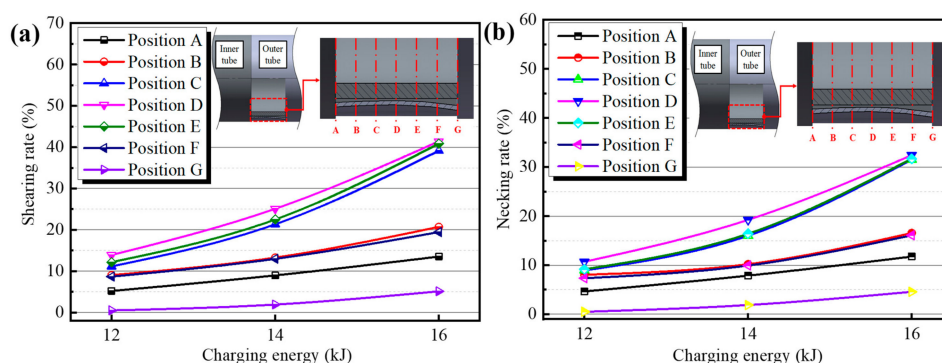


**Figure 11.** Detailed deformation of different positions under different discharge energies (a) shearing rate, (b) necking rate.

Furthermore, the shearing and necking rates of the two typical sections under different discharge energies were compared as shown in Figure 12. It could be found that the shearing rate was a little bigger than the necking rate on the same position, and the difference increased as the discharge energy increased. Besides, the shearing and necking rate of section A was far less than that of section D. This indicated that the shear and necking rate was lower in the position with small deformation.

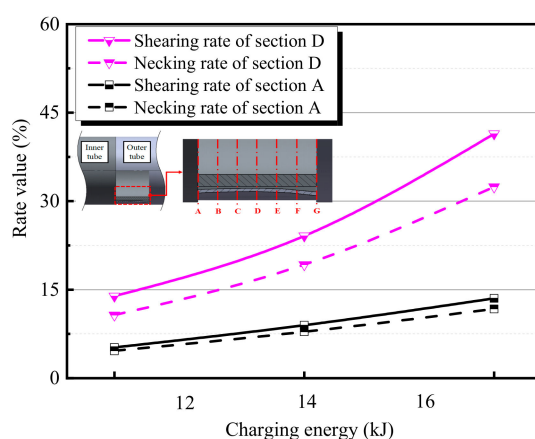


**Figure 12.** Comparison between shearing and necking rate of positions A and D under different charging energies.

### 3.3. Microstructure Observation

The mechanical properties of metal materials after deformation significantly depend on microstructural characteristics. To study the performances of the joint in-depth, microstructure observation of the outer tube filling in the groove was carried out. Figure 13 shows the metallographic structure of the outer tube in detail, which was scrapped by many metallographs. Maximum deformation location (position D) was used for analysis. It could be seen that serious deformation of grains occurred in the region near the edge of the groove by comparing with grains in other regions. In particular, some of the grain was obviously elongated. This could

harden materials in this area, thus increasing the strength of the joint. The grain was deformed in the direction of the arrow in the figure. It was elongated most severely at the edge of the groove, and the degree of elongation decreased with the direction of the arrow. Moreover, a v-shaped thinned area could be seen in the outer wall of the outer tube.

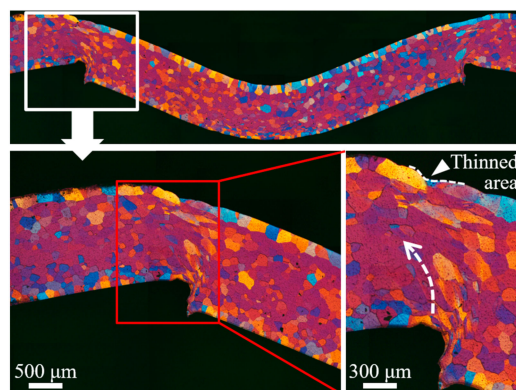


**Figure 13.** Microscopic pictures of position D under 16 kJ.

Under the action of the electromagnetic force, the strain rate during deformation would reach about  $10^{-3} \text{ s}^{-1}$ . The material would flow rapidly to a certain extent at such a high strain rate. When the outer tube was filling into the groove, the materials were sheared along the sidewall of the groove, and severe plastic deformation of the outer tube occurred. At the same time, materials in other areas might flow to the necking area from the nearing region. So the shearing rate was not equal to the necking rate as the results are shown above.

Figure 14 shows local enlargements of thinned area (necking area) in position D under different discharge energies. It could be found that the degree of necking of the outer tube wall became more obvious with the increase of the discharge energy, and v-shaped thinned area could be obviously seen at the discharge energies of 14 and 16 kJ. Especially, some cracks were found in the necking area at the discharge energy of 16 kJ. In addition, grains in the necking area of the joint formed under 12 kJ were almost not elongated compared to the grain of the original outer tube. However, elongated grains could be seen in the necking area of the joints formed under 14 kJ and 16 kJ because of the greater electromagnetic impact force.

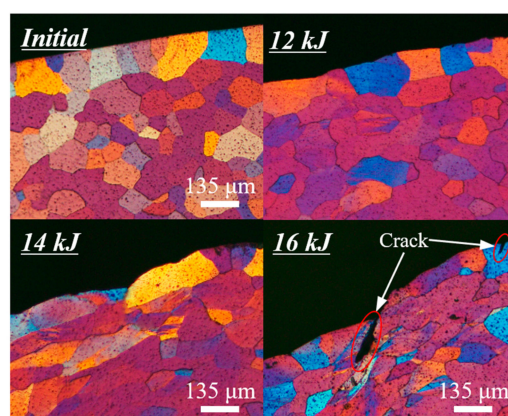


**Figure 14.** Local enlargements of thinned area (necking area) in position D under various discharge energies.

Figure 15 shows local enlargements of the shearing area of position D under different discharge energies. It could be obviously observed that the deformation degree of the shear area increased with the increase of discharge energy. The grains in the shearing area of the

joint formed under 12 kJ were not obviously elongated, while the grains of the joint formed under 14 and 16 kJ were severely stretched.

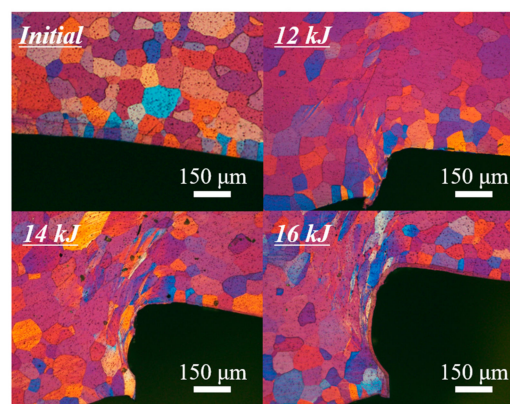


**Figure 15.** Local enlargements of the shearing area of position D under different discharge energies.

In general, under torsional loading, the deformation at the edge of the groove plays an important role in the bearing capacity of the joint. The plastic strengthening of the outer tube at the shearing area makes a contribution. Furthermore, at the discharge energies of 14 and 16 kJ, grains both in the region of the shearing and necking area were elongated in varying degrees. It hardened the materials in these areas, thus improving the strength of the joint. Even some cracks occurred in the region of the necking area, the joint still had enough torsion resistance. Combining the results of torsion tests and the analysis of microstructure observation, the comprehensive performance of the joint at the moderate discharge energy of 14 kJ was optimal.

#### 4. Conclusions

In this work, a new approach for tubes joining using a flat coil was presented. The aluminum-steel crimped joint was manufactured by this method. The conclusions obtained could be drawn as follows:

1. Magnetic pulse crimping using a flat coil could be applicable for torque joints, which is a potentially convenient and flexible method to manufacture tubular components.
2. The torsional failure modes were affected by discharging energies. Joints deformed under 12 kJ were twisted out of the groove, where the torque was about 75% of the outer tube parent material. While the strength of joints deformed under 14 and 16 kJ were higher than the outer tube parent material.
3. The deformation of the outer tube differed along the axial direction of the joint, the biggest of which was in the middle position of the connecting area, then gradually decreasing towards two sides. Moreover, the shearing rate was bigger than the necking rate in every position of the connected region.
4. Severe deformation of grains occurred in the region nearing the edge of the groove. Some cracks occurred in the necking area when the energy was 16 kJ. Combining the results of torsion tests with the microstructure observation, the comprehensive performance of the joint formed under 14 kJ was optimal.

**Author Contributions:** Writing—original draft preparation, Q.L. and H.J.; investigation, Y.Y. and Z.X.; data curation, Z.X. and Y.Y.; methodology, G.L. and J.C.; writing—review and editing, J.C. and G.L.; funding acquisition, H.J. and J.C. All authors have read and agreed to the published version of the manuscript.

**Funding:** This research was funded by National Natural Science Foundation of China, grant number 52175315 and 51975202; China National Postdoctoral Program for Innovative Talents grant number BX20200123; State Key Laboratory of Advanced Design and Manufacturing for Vehicle Body Open fund of Hunan University, grant number 32065009 and Changsha Municipal Natural Science Foundation, grant number kq2014047.

**Institutional Review Board Statement:** Not applicable.

**Informed Consent Statement:** Not applicable.

**Data Availability Statement:** Data sharing is not applicable to this article.

**Conflicts of Interest:** The authors declare no conflict of interest.

## References

1. Jiang, H.; Liao, Y.X.; Gao, S.; Li, G.Y.; Cui, J.J. Comparative study on joining quality of electromagnetic driven self-piecing riveting, adhesive and hybrid joints for Al/steel structure. *Thin Wall. Struct.* **2021**, *164*, 107903. [\[CrossRef\]](#)
2. Jiang, H.; Zeng, C.C.; Li, G.Y.; Cui, J.J. Effect of locking mode on mechanical properties and failure behavior of CFRP/Al electromagnetic riveted joint. *Compos. Struct.* **2020**, *257*, 113162. [\[CrossRef\]](#)
3. Jiang, H.; Li, G.Y.; Zhang, X.; Cui, J.J. Fatigue and failure mechanism in carbon fiber reinforced plastics/aluminum alloy single lap joint produced by electromagnetic riveting technique. *Compos. Sci. Technol.* **2017**, *152*, 1–10. [\[CrossRef\]](#)
4. Qin, Y.F.; Liao, Y.X.; Li, G.Y.; Cui, J.J.; Jiang, H. Numerical Simulation and Parameter Analysis of Electromagnetic Riveting Process for Ti-6Al-4V Titanium Rivet. *Coatings* **2021**, *11*, 878. [\[CrossRef\]](#)
5. Cai, D.; Jin, C.Y.; Liang, J.; Li, G.Y.; Cui, J.J. Multivariate Quadratic Nonlinear Regression Model of the Ultimate Pull-Out Load of Electrohydraulic Expansion Joints Based on Response Surface Methodology. *Coatings* **2021**, *11*, 689. [\[CrossRef\]](#)
6. Cai, D.; Liang, J.; Ou, H.; Li, G.Y.; Cui, J.J. Mechanical properties and joining mechanism of electrohydraulic expansion joints for 6063 aluminum alloy/304 stainless steel thin-walled pipes. *Thin Wall. Struct.* **2021**, *161*, 107427. [\[CrossRef\]](#)
7. Groche, P.; Wohletz, S.; Brenneis, M.; Pabst, C.; Resch, F. Joining by forming—A review on joint mechanisms, applications and future trends. *J. Mater. Process. Technol.* **2014**, *214*, 1972–1994. [\[CrossRef\]](#)
8. Mori, K.; Bay, N.; Fratini, L.; Micari, F.; Tekkaya, A.E. Joining by plastic deformation. *CIRP Ann. Manuf. Technol.* **2013**, *62*, 673–694. [\[CrossRef\]](#)
9. Chen, B.; Chen, K.; Hao, W.; Liang, Z.; Yao, J.; Zhang, L.; Shan, A. Friction stir welding of small-dimension Al3003 and pure Cu pipes. *J. Mater. Process. Technol.* **2015**, *223*, 48–57. [\[CrossRef\]](#)
10. Cho, J.R.; Song, J.I.; Noh, K.T.; Jeon, D.H. Nonlinear finite element analysis of swaging process for automobile power steering hose. *J. Mater. Process. Technol.* **2005**, *170*, 50–57. [\[CrossRef\]](#)
11. Shirgaokar, M.; Cho, H.; Ngaile, G.; Altan, T.; Yu, J.H.; Balconi, J.; Rentfrow, R.; Worrell, W.J. Optimization of mechanical crimping to assemble tubular components. *J. Mater. Process. Technol.* **2004**, *146*, 35–43. [\[CrossRef\]](#)
12. Shirgaokar, M.; Ngaile, G.; Altan, T.; Yu, J.H.; Balconi, J.; Rentfrow, R.; Worrell, W.J. Hydraulic crimping: Application to the assembly of tubular components. *J. Mater. Process. Technol.* **2004**, *146*, 44–51. [\[CrossRef\]](#)
13. Jassim, A.K. Magnetic pulse welding technology. In Proceedings of the 2010 1st International Conference on Energy, Power and Control, New York, NY, USA, 30 November–2 December 2010; Volume 7, pp. 363–373.
14. Deepak, K.; Sachin, D.K.; Arup, N. Experimental investigation of Cu-SS electromagnetically assisted adhesive tube-to-tube joining: Its advantages over electromagnetic crimping. *Int. J. Adhes. Adhes.* **2021**, *109*, 102908.
15. Ashish, K.R.; Sachin, D.K. Numerical simulation and experimental study on electromagnetic crimping of aluminium terminal to copper wire strands. *Electr. Power Syst. Res.* **2018**, *163*, 744–753.
16. Ashish, K.R.; Sachin, D.K. Comparison of different types of coil in Electromagnetic terminal—Wire crimping process: Numerical and experimental analysis. *J. Manuf. Process.* **2018**, *34*, 329–338.
17. Golovashchenko, S. Methodology of design of pulsed electromagnetic joining of tubes. In Proceedings of the TMS Symposium “Innovations in Processing and Manufacturing of Sheet Materials”, New Orleans, LA, USA, 1 February 2001; pp. 283–299.
18. Park, Y.B.; Kim, H.Y.; Oh, S.I. Design of axial/torque joint made by electromagnetic forming. *Thin-Walled Struct.* **2005**, *43*, 826–844. [\[CrossRef\]](#)
19. Weddeling, C.; Woodward, S.T.; Marr, M.; Nellesen, J.; Psyk, V.; Tekkaya, A.E.; Tillmann, W. Influence of groove characteristics on strength of form-fit joints. *J. Mater. Process. Technol.* **2011**, *211*, 925–935. [\[CrossRef\]](#)
20. Weddeling, C.; Walter, V.; Haupt, P.; Tekkaya, A.E.; Schulze, V.; Weidenmann, K.A. Joining zone design for electromagnetically crimped connections. *J. Mater. Process. Technol.* **2015**, *225*, 240–261. [\[CrossRef\]](#)
21. Geng, H.H.; Mao, J.Q.; Zhang, X.; Li, G.Y.; Cui, J.J. Strain rate sensitivity of Al-Fe magnetic pulse welds. *J. Mater. Process. Technol.* **2018**, *262*, 1–10. [\[CrossRef\]](#)